Check for updates

RESEARCH ARTICLE

NANO · MICRO small
www.small-journal.com

Metal–Organic Framework as a New Type of Magnetothermally-Triggered On-Demand Release Carrier

Xueying Ge, Jeotikanta Mohapatra, Enya Silva, Guihua He, Lingshan Gong, Tengteng Lyu, Richa P. Madhogaria, Xin Zhao, Yuchuan Cheng, Abdullah M. Al-Enizi, Ayman Nafady, Jian Tian, J. Ping Liu, Manh-Huong Phan, Francesca Taraballi, Roderic I. Pettigrew, and Shengqian Ma**

The development of external stimuli-controlled payload systems has been sought after with increasing interest toward magnetothermally-triggered drug release (MTDR) carriers due to their non-invasive features. However, current MTDR carriers present several limitations, such as poor heating efficiency caused by the aggregation of iron oxide nanoparticles (IONPs) or the presence of antiferromagnetic phases which affect their efficiency. Herein, a novel MTDR carrier is developed using a controlled encapsulation method that fully fixes and confines IONPs of various sizes within the metal–organic frameworks (MOFs). This novel carrier preserves the MOF's morphology, porosity, and IONP segregation, while enhances heating efficiency through the oxidation of antiferromagnetic phases in IONPs during encapsulation. It also features a magnetothermally-responsive nanobrush that is stimulated by an alternating magnetic field to enable on-demand drug release. The novel carrier shows improved heating, which has potential applications as contrast agents and for combined chemo and magnetic hyperthermia therapy. It holds a great promise for magneto-thermally modulated drug dosing at tumor sites, making it an exciting avenue for cancer treatment.

1. Introduction

Non-invasive drug release technology controlled by an external stimulus offers the potential to reduce systemic toxicity and improve therapeutic efficacy.[1] Magnetothermally-triggered drug release (MTDR) systems have sparked a rapidly growing interest due to the ability to locate targets deeply inside a bio-system and potentially reducing off-target adverse effects.[2] It is worth noting that the MTDR systems require both a magnetic heating mediator and a carrier with magnetothermally-responsive nanocoating to achieve on-demand drug release control. Iron oxide nanoparticles (IONPs) owing to their biocompatibility and availability, have been extensively studied as localized magnetic heating mediators in the past 20 years.[3] The recent approval of IONPs as a medical device for hyperthermia treatment of glioblastoma multiforme brain tumors in Europe, along with ongoing clinical trials for their use in the treatment of prostate and pancreatic cancers, underscores the promising potential of IONPs as magnetic heating mediators for clinical translation in the MTDR system.[4]

The most commonly used MTDR carriers are mesoporous silica nanomaterials,[5] graphene-based nanomaterials, and polymers.[6] However, their relatively poor heat transfer efficiency caused by IONP aggregation and the existence of antiferromagnetic phase[3d,7] presents translational challenges for effective drug release. This can result in inadequate heat to activate the nanocoating for on/off control of drug release, or require the integration of highly concentrated IONPs imposing possible concomitant adverse side

X. Ge, L. Gong, T. Lyu, S. Ma
Department of Chemistry
University of North Texas
Denton, Texas 76201, USA
E-mail: Shengqian.ma@unt.edu

X. Ge, R. I. Pettigrew
Engineering Medicine (EnMed)
Texas A&M University and Houston Methodist Hospital
Houston, Texas 77030, USA

J. Mohapatra, J. P. Liu
Department of Physics
The University of Texas at Arlington
Arlington, Texas 76019, USA

E. Silva, R. P. Madhogaria, M.-H. Phan
Department of Physics
University of South Florida
Tampa, Florida 33620, USA

G. He, J. Tian
Key Laboratory of Combinatorial Biosynthesis and Drug Discovery (MOE)
Hubei Province Engineering and Technology Research Center for Fluorinated Pharmaceuticals
School of Pharmaceutical Sciences
Wuhan University
Wuhan 430071, P. R. China
E-mail: jian.tian@whu.edu.cn

The ORCID identification number(s) for the author(s) of this article can be found under https://doi.org/10.1002/smll.202306940

DOI: 10.1002/smll.202306940

 © 2023 Wiley-VCH GmbH

effects.[8] To circumvent this issue, new types of carriers that can fix and disperse IONPs are needed to prevent aggregation and minimize IONP encapsulation thus optimizing the heating efficiency.[3d] Furthermore, these carriers with enhanced heating activity should be able to be grafted with magnetothermally-responsive nanocoating, which would enable on-demand drug release.

Notably, metal–organic frameworks (MOFs) have displayed advantages for their potential use as carriers in drug delivery field due to their high surface areas, proper pore size dimensions, and functionalized walls.[9] By pre-designing and/or post-modifying the linkers and secondary building units (SBUs), MOFs can be further modified with different controllable nanocoatings.[10] Given their highly porous nature and ease in functionalization, MOFs are appealing candidates as MTDR carriers.[11] Their well-defined pore structure together with multiple binding sites on the pore walls offer inherent environments for spatial confinement and segregation of incorporated nanoparticles,[12] thereby making MOFs suitable carriers for fixing and encapsulating IONPs. Previous studies explored IONPs/MOF composites[13] for potential use in drug delivery and hyperthermia treatment,[14] showing the feasibility of these nanocomposite materials. However, there are still several challenges that need to be addressed for practical deployment and potential clinical utility. First, the efficient transfer of electromagnetic energy to heat requires the segregation of IONPs to prevent their fusion and agglomeration. However, in the existing IONPs/MOF composites, agglomeration is frequently observed despite the use of surface functional groups such as polyvinylpyrrolidone (PVP), mercaptoacetic acid (MAA), and poly(acrylic acid) (PAA), which are commonly utilized to assist in the construction of the IONPs@MOF nanocomposites (@ refers to core-shell structure), due to their low and reversible ligand exchange process.[15] Second, maintaining the well-defined pore structure of MOF after fixing the encapsulated IONPs within the MOF matrix is difficult to achieve because the existing IONPs/MOF composites that hold the IONPs in place tend to retain the shape of the pristine IONPs.[12a,13a,14a,b,f,16] Third, existing IONPs/MOF composites make the advantage of alternating magnetic field (AMF)-triggered drug release over traditional temperature-triggered ones (i.e., drug-releasing medium heated by hotplates) remains elusive.[14e,f,17] Notably, the temperature at the nanoparticle surface (also known as local temperature) is different from and always higher than the macroscopic temperature recorded in the IONP dispersion medium.[18] The existing IONPs/MOF composites are often encapsulated with highly concentrated IONPs to increase the macroscopic heating temperature under a magnetic field. However, this causes the IONPs to heavily aggregate, lose the MOF's porosity and morphology, and ultimately reduce their heating efficiency. This can impede the IONPs/MOF nanocomposites' biomedical application. Instead, ideal composites should produce the maximum heat with minimal loading IONPs,[3d] even if the macroscopic temperature is unperceived. Therefore, drug release should only occur under AMF stimuli, regardless of the lack of a rise in the macroscopic temperature. Fourth, magnetothermally-responsive nanocoatings are essential for the MTDR on-demand system to control the on/off release avoiding drug leaching. This has not been achieved in the existing IONPs/MOF composites.[14e,17,19]

To address the aforementioned challenges, our strategy focuses on the spatial distribution of IONPs within a MOF matrix, creating an intimate contact between IONPs and MOF matrix. The intimate contact prevents the agglomeration of IONPs and facilitates heat transfer, resulting in an overall improved heating efficiency for IONPs/MOF composites. As a proof of concept, IONPs are obtained through the high-temperature thermolysis procedures[20] with oleic acid (OA) grafted on the exterior surface (denoted as IONP-OA), which is subsequently oxidized by Lemieux-von Rudloff reagent to become azelaic acid (COOH)[21] (denoted as IONP-COOH), facilitating the formation of IONPs@MOF nanocomposites. The MOF, UiO-66-NH_2 was selected for fabricating the magnetothermal nanocomposite considering its rapid nucleation, water stability, and the existence of structure defects.[22] As shown in **Figure 1**, due to the presence of azelaic acid, IONPs and ligand can both coordinate with metal ions/clusters to form IONPs@UiO-66-NH_2 (denoted as MFC (magnetic framework composites)) with IONPs uniformly incorporated and fixed within the UiO-66-NH_2 matrix (**Figure 2a**). Such synthesis method provides an intimate contact between MOF and IONPs, allowing the retention of the porosity of MOF, segregation of the IONPs, and also the preservation of the superparamagnetic properties of IONPs. Moreover, the impurity and defects in IONP-COOH nanoparticle[23] structures can be oxidized to the pure magnetite[24] during the MFC nanocomposite synthesis, which affords the increase in magnetization values therefore facilitating the heat transfer to enhance overall heating efficiency in comparison with the as-synthesized IONPs. It is worth mentioning, compared to other IONPs@UiO-66 nanocomposites,[14a,b,16f] the designed MFC herein represents the first example of nanocomposite with MOF morphology preserved and the IONPs fully fixed within the MOF matrix, thereby making it a promising candidate as MTDR carrier.

To achieve MTDR, a thermo-responsive polymer (or nanobrush), Poly(*N*-isopropylacrylamide) (PNIPAM),[25] which undergoes a conformational change at the phase transition temperature,[26] and collapses from an extended brush[27] when the temperature is higher than the phase transition temperature.[28] We aim to covalently anchor this polymer to

X. Zhao
J. Mike Walker '66 Department of Mechanical Engineering
Texas A&M University
College Station, TX 77843, USA
Y. Cheng
Zhejiang Key Laboratory of Additive Manufacturing Materials
Ningbo Institute of Material Technology and Engineering
Chinese Academy of Sciences
Ningbo 315201, P. R. China
A. M. Al-Enizi, A. Nafady
Department of Chemistry
College of Science
King Saud University
Riyadh 11451, Saudi Arabia
F. Taraballi
Center for Musculoskeletal Regeneration
Orthopedics and Sports Medicine
Houston Methodist Hospital
Houston Methodist Academic Institute
Houston, Texas 77030, USA

© 2023 Wiley-VCH GmbH

16136829, 2024, 12, Downloaded from https://onlinelibrary.wiley.com/doi/10.1002/smll.202306940 by University Of Toronto Librarie, Wiley Online Library on [25/03/2024]. See the Terms and Conditions (https://onlinelibrary.wiley.com/terms-and-conditions) on Wiley Online Library for rules of use; OA articles are governed by the applicable Creative Commons License

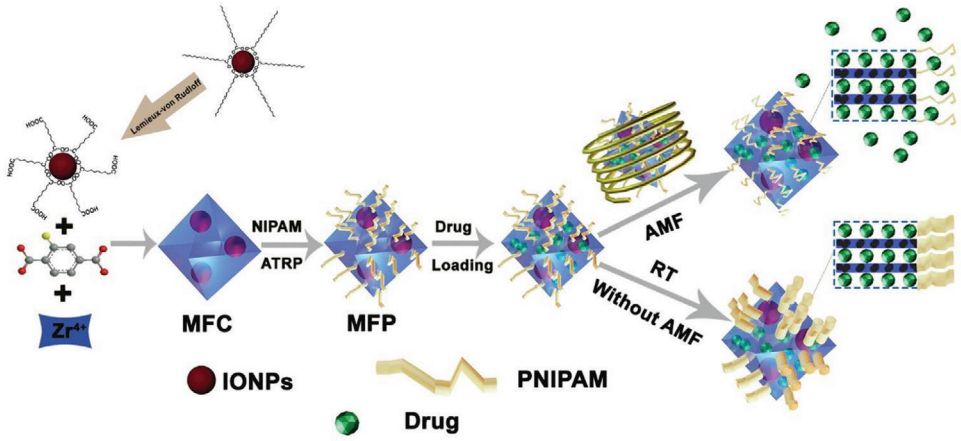

Figure 1. Proof-of-concept design. Spatial incorporation of IONPs in the UiO-66-NH_2 matrix and PNIPAM is grafted on the exterior surface of UiO-66-NH_2 through an ATRP method. The drug is released at the PNIPAM's collapsing state under AMF, whereas the drug is retained within MOF pore at the PNIPAM's hydrated state at RT.

the MFC support (denoted as MFP, magnetic framework polymer) through atom transfer radical polymerization (ATRP),[29] a useful modification method[30] that is only restricted to the surface of MFC. Hence, there are no free polymers formed in solution to clog the MOF pores, as compared to the polymer "grafting-to" approach.[31] At room temperature (RT) without AMF, the polymer is extended and hydrated, exhibiting a gate-closing behavior, and preventing the drug release, whereas at an external AMF (or high temperature) it becomes collapsed, showing a gate-opening behavior thus allowing the release of the drug. Therefore, with the application of AMF, the heat generated by the IONPs well-dispersed in the MOF matrix will then be efficiently and evenly transferred onto the surface of IONPs@MOF. This renders a conformational change of the nanobrush thus opening the passage to achieve the on-demand drug release. The performance of the IONPs@MOF has been

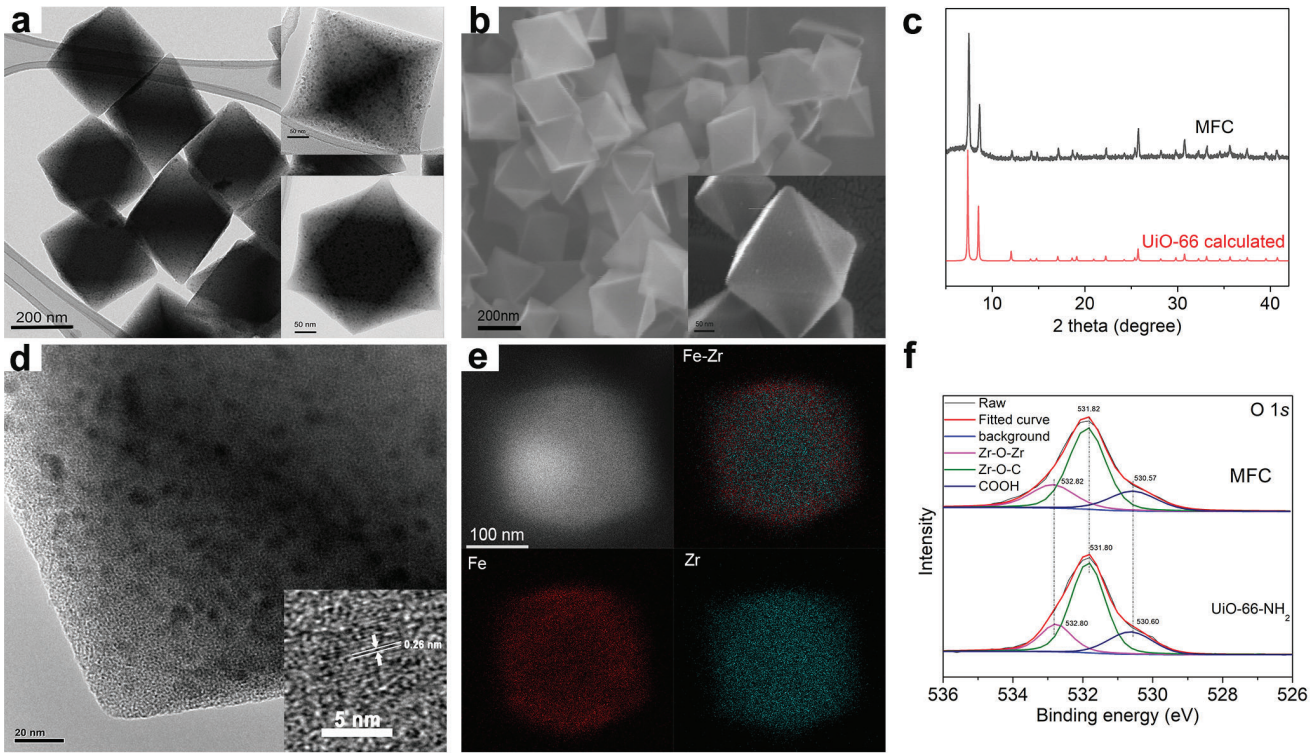

Figure 2. a) SEM and b) TEM images of MFC nanoparticles; Insert TEM images (a) and SEM images (b) of a single MFC nanostructure; c) PXRD pattern of MFC; d) a magnified TEM image and high-resolution TEM (HR-TEM) image (insert) of MFC; e) a scanning TEM (STEM) image and the corresponding element mapping of MFC; f) XPS spectra of O 1s XPS for UiO-66-NH_2 and MFC.

© 2023 Wiley-VCH GmbH

16136829, 2024, 12, Downloaded from https://onlinelibrary.wiley.com/doi/10.1002/smll.202306940 by University Of Toronto Librarie, Wiley Online Library on [25/03/2024]. See the Terms and Conditions (https://onlinelibrary.wiley.com/terms-and-conditions) on Wiley Online Library for rules of use; OA articles are governed by the applicable Creative Commons License

demonstrated in an in vitro imaging experiment and chemo-hyperthermia therapy in cell studies. Interestingly, PNIPAM functionalization can improve magnetothermal response, which may be related to the decreased inter-particle interaction, thus leading to enhanced susceptibility loss due to the Brownian relaxation.[3b,c,32] The enhanced heating efficiencies for MFC and MFP nanocomposites highlight the superiority of MOF as a carrier to fix IONPs as compared with other carriers (Table S1, Supporting Information), thus satisfying the criterion for maximizing the specific absorption rate (SAR) with the minimal amount of IONPs.[33]

2. Results and Discussion

2.1. Fabrication of the Magnetothermal Nanocomposites

IONPs were synthesized using a thermal decomposition method, since high temperature of the chemical reaction favors the formation of monodisperse magnetic nanocrystals with high heating efficiency.[3d,20] The resulting nanoparticles, capped with hydrophobic organic ligand (OA), were synthesized, followed by conversion into carboxylic acid-functionalized IONPs using the Lemieux-von Rudloff reagent[21] (Figure S1, Supporting Information shows the approach of converting IONP-OA to IONP-COOH), which can provide coordination groups to assist the assembly with MOFs. As shown in Figure S2a (Supporting Information), IONP-COOH nanoparticles showed a highly uniform and well-defined spherical morphology with a diameter of 9.4±0.9 nm (Figure S2b, Supporting Information). The powder X-ray diffraction (PXRD) patterns (Figure S2c, Supporting Information) of IONP-COOH showed that the synthesized nanoparticles are not pure phase magnetite, which caused the reduction of the magnetization value. After being treated by the synthesized solution of MFC nanocomposites, the recorded PXRD confirms that they are completely converted to magnetite phase. The preparation of pure magnetite phase in MFC sample could lead to a high magnetic moment, which is desirable for their use in MTDR. The carboxylic acid coating layer was confirmed by Fourier transform infrared (FTIR)[34] (Figure S3, Supporting Information). Table S2 (Supporting Information) shows the dynamic light scattering and zeta potential for IONP-COOH and IONP-OA. As shown in Figure S4 (Supporting Information), the IONP-COOH nanoparticles repel against each other due to the presence of negatively charged carboxylic groups on their surfaces,[3a] which become well-dispersed in the DMF solution containing the precursors of UiO-66-NH_2. The IONP-COOH nanoparticles can assist the growth of MOFs since carboxylic groups on their surface coordinate with the Zr ions in the solution as the organic linkers. As can be seen from the transmission electron microscopy (TEM) and scanning electron microscope (SEM) images in Figure 2a,b, the as-synthesized MFC nanocomposites have an octahedral geometry with a side length of 256±39 nm (Figure S5, Supporting Information), and the IONP-COOH nanoparticles are homogeneously incorporated and fixed within UiO-66-NH_2 framework as evidenced by TEM (Figure 2a,d) along with energy-dispersive X-ray (EDX) analysis (Figure S6, Supporting Information), and the elemental mapping analysis (Figure 2e). The shift in X-ray photoelectron spectroscopy (XPS) spectra of O 1*s* further confirmed the presence of IONPs and the functionalized group, azelaic acid, within MFC structure when compared with UiO-66-NH_2 (Figure 2f).[35] A detailed analysis of the cores within the MOF structure by HRTEM showed that the lattice fringe was ≈0.26 nm (Figure 2d insert graph), corresponding to the (311) plane of the magnetite (Figure S2a, Supporting Information). Large-scale SEM image (Figure S5, Supporting Information) and STEM (Figure 2e) were also taken, which proves that there are no IONP-COOH nanoparticles on the exterior surface of UiO-66-NH_2. To trace the formation process of the MFC, the reaction vials were taken out at the interval time and then analyzed by TEM and PXRD (Figures S7,S8, Supporting Information). Within 30 min, UiO-66-NH_2 was formed as confirmed by PXRD, with only one IONP-COOH nanoparticle incorporated into a MOF morphology, whereas the other nanoparticles were observed on the TEM copper grid. As the reaction proceeded, more IONP-COOH nanoparticles were encapsulated into MOFs. Finally, the MFC nanocomposites were formed, with all IONP-COOH nanoparticles uniformly incorporated and fixed within the MOF frameworks. These results indicate that the confinement process of IONPs does not depend on heterogeneous nucleation. Nevertheless, it relies on the continuous adsorbing of IONPs onto the gradually growing surfaces of the MOF crystal, as compared to the previously reported synthesis method of growing MOF crystal around the pre-synthesized IONPs.[13a,14b,15a,16c,i,j,36] Intrigued by these findings, different amounts of IONP-COOH nanoparticles were chosen for incorporation within UiO-66-NH_2 matrix, which were characterized by SEM (Figure S9, Supporting Information) and inductively coupled plasma-optical emission spectrometry (ICP-OES) (Figure S10 and Table S3, Supporting Information). As the amount of IONP-COOH nanoparticles increases, the IONP-COOH nanoparticles will be gradually attached to the exterior surface of UiO-66-NH_2, given that only a certain number of IONP-COOH nanoparticles could be incorporated and fixed within the MFC nanocomposites. According to ICP-OES (Table S3, Supporting Information), the maximum incorporation ratio of Fe is ≈1.71 wt.%. The PXRD patterns (Figure 2c) reveal that the confinement method of IONPs could retain the structure of MOF even as the mass of IONPs increased (Figure S11, Supporting Information). Interestingly, the final MFC nanocomposites' pattern matched well with the calculated UiO-66 without the observation of any broadened peaks of IONP-COOH nanoparticles, indicating that the final product maintains the MOF's morphology. N_2 sorption isotherms of MFC at 77K revealed that as compared with pristine UiO-66-NH_2 (Figure S12, Supporting Information, S_{BET} is 1202 $m^2\ g^{-1}$), the Brunauer–Emmett-Teller surface area (S_{BET}) reduced to 780 $m^2\ g^{-1}$ (Figure 4a) due to the incorporation of non-porous IONP-COOH nanoparticles; with the increasing amount of IONP-COOH nanoparticles, the S_{BET} of IONPs@UiO-66-NH_2 gradually decreased as shown in Figure S12 (Supporting Information).

2.2. Magnetization Curves

The magnetization versus magnetic field *(M–H)* curves of MFC, IONP-COOH, and treated IONP-COOH nanoparticles were measured by a Vibrating Sample Magnetometer (VSM) equipped with the Physical Property Measurement System from Quantum

© 2023 Wiley-VCH GmbH

16136829, 2024, 12, Downloaded from https://onlinelibrary.wiley.com/doi/10.1002/smll.202306940 by University Of Toronto Librarie, Wiley Online Library on [25/03/2024]. See the Terms and Conditions (https://onlinelibrary.wiley.com/terms-and-conditions) on Wiley Online Library for rules of use; OA articles are governed by the applicable Creative Commons License

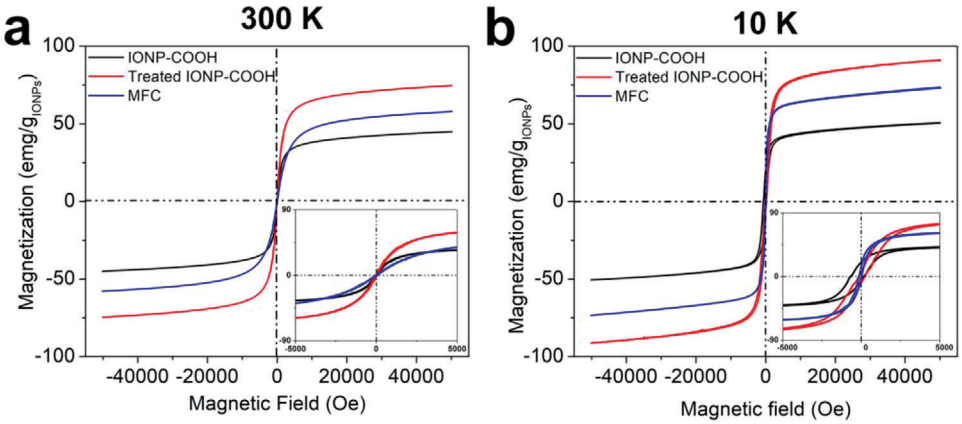

Figure 3. *M–H* curves taken at a) 300 K and b) 10 K. Insert graphs are the low field enlargement at 300 K (a) and 10 K (b) to evaluate the superparamagnetic characteristics and exchange bias for IONP-COOH, treated IONP-COOH, and MFC nanoparticles.

Design. It should be noted that the synthesis of "treated IONP-COOH" follows the same conditions used for IONP-COOH nanoparticles encapsulation into MOF structure, but notably excludes the addition of the metal and ligand components. This distinction aids in elucidating the encapsulation mechanism. A detailed procedure can be found in the Supporting Information. As shown in **Figure 3**a, the *M–H* curves at 300 K show no magnetic hysteresis, indicating that all three samples are superparamagnetic.[37] The treated IONP-COOH nanoparticles showed the highest saturation magnetization (*Ms*) values (≈74.6 emu/g_{IONPs}) compared with IONP-COOH (≈45 emu/g_{IONPs}) and the MFC (≈58 emu/g_{IONPs}). As suggested by the PXRD analysis (Figure S2, Supporting Information), the increased magnetization in treated IONP-COOH and MFC is related to the formation of the pure magnetite phase in these two samples. To further understand their magnetic properties, the field-cooled magnetization curves at 10 K were collected, as depicted in Figure 3b. An exchange bias (H_{EB}≈275 Oe) and coercivity (H_c≈411 Oe) were presented in the hysteresis loop of IONP-COOH. In contrast, no H_{EB} and H_c reduced to 75 Oe were observed for MFC, which can be ascribed to the formation of the pure magnetite phase. The pronounced exchange bias in IONP-COOH is related to the antiferromagnetic/ferrimagnetic exchange interactions.[38] It was suggested that the high *Ms* value causes the high hyperthermia response. From the *M–H* curve in Figure 3, *Ms* values of MFC are lower than the treated IONP-COOH nanoparticles, but higher than the original IONP-COOH nanoparticles. The reduction of MFC's *Ms* value in comparison with the treated samples is likely due to the surface-spin canting effect.[39]

2.3. Encapsulation of Different-Sized IONPs

To maximize the benefit of this encapsulating strategy, different-sized IONP-COOH nanoparticles (10.7±0.5 nm and 14±0.8 nm) were encapsulated into MOFs as shown in Figure S13a,b (Supporting Information). The synthesis of those nanoparticles was similar to the 9.4±0.9 nm one, except for the use of a different amount of iron oleate. As shown in Figure S13c,d (Supporting Information), different-sized IONP-COOH nanoparticles uniformly dispersed and fixed with MOF frameworks were obtained. Interestingly, all the MFC nanocomposites showed higher *Ms* values compared with IONP-COOH itself (Figure S13e,f, Supporting Information), indicating that the MOF synthesis solution can be used to oxidize the impurity and defect phase in different-sized IONPs to the magnetite phase. Therefore, this encapsulation method holds great promise for fixing different hydrophobic nanoparticles within MOF matrix in a non-agglomerated manner, possibly with enhanced or new properties compared to the parent MOF and nanoparticles.

2.4. Grafting Thermally-Responsive Polymer

The AMF-responsive features of the MFC nanocomposites are rendered by grafting the PNIPAM polymer on the exterior surface of MFCs through ATRP methods. Initially, α-bromoisobutyryl bromide (BIBB) was grafted onto the surface of UiO-66-NH_2 as the initiator for the ATRP-mediated process (Figure S14, Supporting Information). Subsequently, the polymer growth was conducted by immersing the MFC in a mixed solution containing both NIPAM (*N*-isopropylacrylamide) monomer and an appropriate catalyst for 2 h. The grafting content of PNIPAM moiety monitored by elemental analysis and ICP-OES was ≈21.9% (Tables S4,S5, Supporting Information). Figure S15a (Supporting Information) shows the XPS spectra of MFC and MFP with the observation of a new peak ≈70 eV in MFP which is associated with Br 3d,[29a] indicative of the successful grafting of the PNIPAM polymer on the exterior surface of MFC. The TGA profile of MFP suggested a constant weight loss compared with MFC due to the presence of PNIPAM (Figure S16, Supporting Information). N_2 sorption isotherm of MFP at 77K shows a reduction in S_{BET} to 480 m^2 g^{-1} (**Figure 4**a) due to the mass of PNIPAM, indicating that most of the MOF pore remained intact after functionalized with PNIPAM. There was no noticeable change in the pore size distribution (Figure S17, Supporting Information). The MOF crystal structure and the IONPs fixed within MFP remained unaltered after functionalized with PNIPAM, as suggested by the combined studies of PXRD (Figure 4b), XPS (Figure S15b, Supporting Information) and

© 2023 Wiley-VCH GmbH

16136829, 2024, 12, Downloaded from https://onlinelibrary.wiley.com/doi/10.1002/smll.202306940 by University Of Toronto Librarie, Wiley Online Library on [25/03/2024]. See the Terms and Conditions (https://onlinelibrary.wiley.com/terms-and-conditions) on Wiley Online Library for rules of use; OA articles are governed by the applicable Creative Commons License

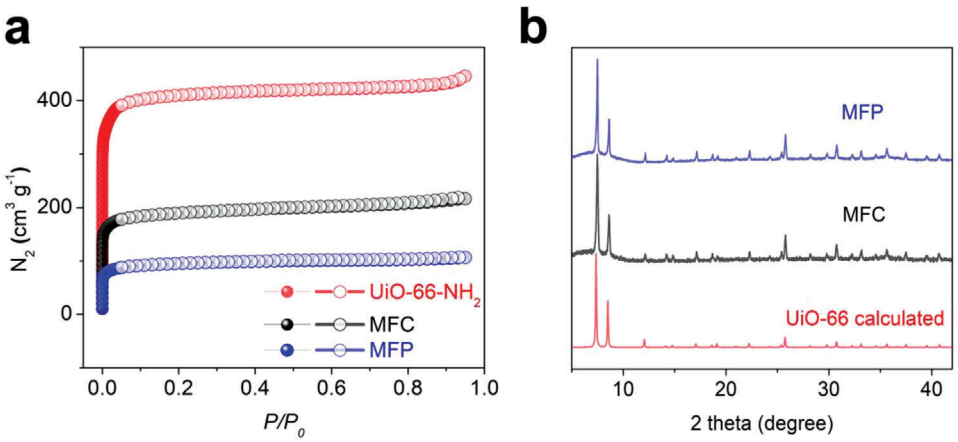

Figure 4. a) N_2 adsorption-desorption isotherms of MFC (black line) and MFP (blue line) compared with UiO-66-NH_2 (solid one: adsorption; empty one: desorption); b) PXRD pattern of MFC (black line) and MFP (blue line).

TEM (Figure S18, Supporting Information). As shown in Figure S19 (Supporting Information), the C–H stretching at 2910 and 2952 cm^{-1}, originating from PNIPAM structure[25] can be clearly observed in MFP. The spectra for MFC clearly exhibit the N-H bending at 1656 cm^{-1} associated with the primary amine and C–N stretching at 1336 cm^{-1} for the aromatic primary amines.[40] However, these characteristic peaks are noticeably absent in the spectra for MFP, demonstrating successful grafting of PNIPAM onto the surface of MFC.

2.5. Magnetothermal Performance

To evaluate the magnetothermal performance of these nanocomposites, their SAR[41] values were determined from calorimetric measurements using an Ambrell Easyheat LI 3542 system that provides AMFs at 310 kHz with field amplitudes up to 800 Oe. **Figure** 5a–c show the typical heating curves of the a) IONP-COOH, b) MFC, c) MFP nanoparticles at different alternating current (AC) magnetic fields. It can be observed in these figures that the heating rates progressively increase with the enhancement of AC magnetic fields. It is worth mentioning that upon the application of an 800 Oe field, the temperature of MFP could easily reach 40–45 °C, at which the cancer cells are more sensitive than healthy ones,[42] thus resulting in selective thermal destruction.[43] The SAR values were calculated by considering the slopes of the heating curves from Figure 5a–c using the method described in the Calculation part in Supporting Information. It is interesting to note that among the samples investigated, the MFP nanocomposites show the highest value for all applied AC fields (Figure 5d). This can be ascribed to that the intimate contact between MOF and IONPs together with the PNIPAM functionalization restricts the diffusion and aggregation of IONPs as well as the high *Ms* value of the IONP-COOH nanoparticles within the MOF framework, thereby leading to an enhanced magnetothermal response. In order to explore the further application in the cell condition, MFC under an AC magnetic field (221 kHz, 400 Oe) was found to have a higher SAR value (850 emu/g_{Fe}) than that of IONP-COOH at the same Fe concentration (Figure S20, Supporting Information).

2.6. Drug Loading and Release

The porous feature and enhanced SAR values prompted us to investigate MFP for use in MTDR systems. 5-Fluorouracil (5-FU), an anti-cancer drug,[44] was selected to be loaded into the MFP nanocomposites considering its suitable size (5.3 Å × 4.9 Å)[45] fitting into MFP cavities (Figure S17, Supporting Information). A loading efficiency of 13.1 wt.% for 5-FU was determined from UV-vis spectrum measurement (Figure S22, Supporting Information). PXRD and SEM (Figure S23, Supporting Information) studies on 5-FU@MFP revealed the intactness for the structure of MFP after 5-FU was loaded into MFP's pore, which led to a decrease in S_{BET} to 350 m^2 g^{-1} as estimated by N_2 sorption isotherms at 77 K (Figure S24, Supporting Information). 5-FU can be readily released from MFP's pores through the conformational change of PNIPAM induced by the heat that is generated from IONPs under AMF. AMF (310 kHz and 800 Oe) and UV–vis absorption spectrometer were used to monitor the release profile of 5-FU from the MFP. As shown in **Figure** 6a, 80% of 5-FU was observed to release from MFP nanocomposites within 40 min when applying AMF. On the contrary, just 16% of 5-FU was released at RT in the absence of an AMF. Interestingly, only 20% of 5-FU was released when the release medium was heated up to 50 °C using the oil bath, although the solution temperature was kept the same with that under the AMF. This important finding implies that local heating at the MFP nanocomposite's surface is vital to improve the release efficiency of 5-FU.[18a] The 5-FU released from MFP over a longer period at RT and 50 °C is also monitored from Figure S25a (Supporting Information), showing only 32% of 5-FU was released for over 4 h at 50°C. This indicates that AMF could dramatically enhance the drug release rate, as compared to the temperature-controlled drug release. Interestingly, as shown in Figure S25b (Supporting Information), within 200 min, over 50% of 5-FU was released from MFC carriers at RT, suggesting that PNIPAM could inhibit drug release when grafted on the exterior surface of MFC. This further proved that PNIPAM could be used as magnetothermally-responsive nanobrush for AMF-triggered drug release. The collected PXRD patterns showed that MFP did not decompose after 5-FU release subject to AMF or the oil bath (Figure S26, Supporting Information),

© 2023 Wiley-VCH GmbH

16136829, 2024, 12, Downloaded from https://onlinelibrary.wiley.com/doi/10.1002/smll.202306940 by University Of Toronto Librarie, Wiley Online Library on [25/03/2024]. See the Terms and Conditions (https://onlinelibrary.wiley.com/terms-and-conditions) on Wiley Online Library for rules of use; OA articles are governed by the applicable Creative Commons License

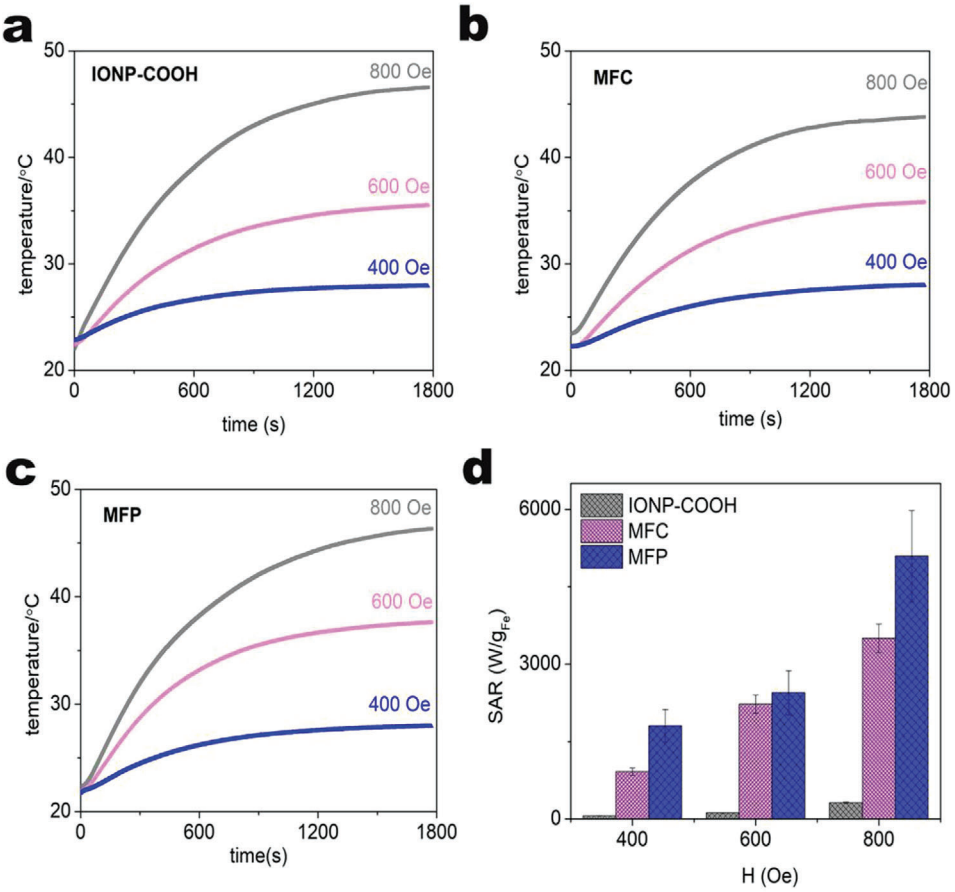

Figure 5. Heating curves of 1 mg mL^{-1} nanoparticle water dispersion: a) IONP-COOH (353.3 μg Fe/mL), b) MFC (17.1 μg Fe/mL), c) MFP (13.4 μg Fe/mL) under different AC magnetic fields at a constant frequency, f = 310 kHz; d) SAR value, which is expressed in watt per gram of Fe (W/g$_{Fe}$), of IONP-COOH, MFC and MFP nanoparticles obtained from (a), (b), and (c). Data are expressed as means ± SD (n = 3).

suggesting 5-FU could be substantially released from MFP's pore under AMF and temperature.

2.7. Extended Application of the Nanocomposites in Imaging and Cells

The successful fixing and dispersing of IONPs within a MOF matrix offers opportunities for its use as a contrast agent. The transverse relaxivity (r_2) of MFC is determined to be ≈507.35 mM^{-1} s^{-1} (Figure 6c), which is higher than those of recently reported porous material-based T_2-weighted contrast agents,[14e,46] such as Fe_3O_4@UiO-66 (255.87 mM^{-1} s^{-1}),[14b] Fe_3O_4@C@MIL-101(Fe)[16c] (352.45 mM^{-1} s^{-1}), γ-SD/PLL (269.3 mM^{-1} s^{-1})[14e] and Fe_3O_4@C@ZIF-8 (331.79 mM^{-1} s^{-1}),[17] suggesting its potential as a magnetic resonance imaging (MRI) contrast agent.[47] The observed r_2 is nearly eleven times higher than the synthesized IONP-COOH nanoparticles (~44.2 mM^{-1} s^{-1} (Figure S27, Supporting Information)) and five times higher than the ferumoxytol,[48] which is related to the high saturation magnetization value and large outer-sphere effect together with the intimate contact of incorporated IONP-COOH nanoparticles within the MOF matrix, highlighting the great potential of MFC in T_2-weighted MRI.

Our nanocomposites also have the potential to promote cancer cell toxicity when stimulated by an AMF. The experiments toward the in vitro cell viability of MFC with three different cell lines: fibroblast cells (L-929), colorectal cancer cells (CT-26), and breast cancer cells (4T-1), were conducted to evaluate its biocompatibility. In Figure 6b, the as-synthesized MFC had minimal cytotoxicity to 4T-1, L-929, and CT-26 cell lines, with almost 85%, 78%, and 93% cell viability even at 200 μg mL^{-1}. The cell viability of 4T-1 cells for long incubation time with IONP-COOH and MFC nanoparticles (48 and 72 h) was also investigated (Figure S28a, Supporting Information). The structure for MFC is still intact after immersing into cell culture solution for over 48 h (Figure S28b, Supporting Information). This demonstrates that fixing IONPs within the UiO-66-NH_2 matrix can enhance the stability of UiO-66-NH_2 due to their intimate contact[49]. Therefore, MFC could be a promising MTDR system with good biocompatibility. The magnetic hyperthermia treatment effect for the 4T-1 cell is shown in Figure S29 (Supporting Information). It can be seen that the MFC significantly reduced the cell viability from 92% to 72% as the AC magnetic field increased from 400 to 800 Oe for a treatment time of 5 min. Furthermore, the cell viability markedly

© 2023 Wiley-VCH GmbH

16136829, 2024, 12, Downloaded from https://onlinelibrary.wiley.com/doi/10.1002/smll.202306940 by University Of Toronto Librarie, Wiley Online Library on [25/03/2024]. See the Terms and Conditions (https://onlinelibrary.wiley.com/terms-and-conditions) on Wiley Online Library for rules of use; OA articles are governed by the applicable Creative Commons License

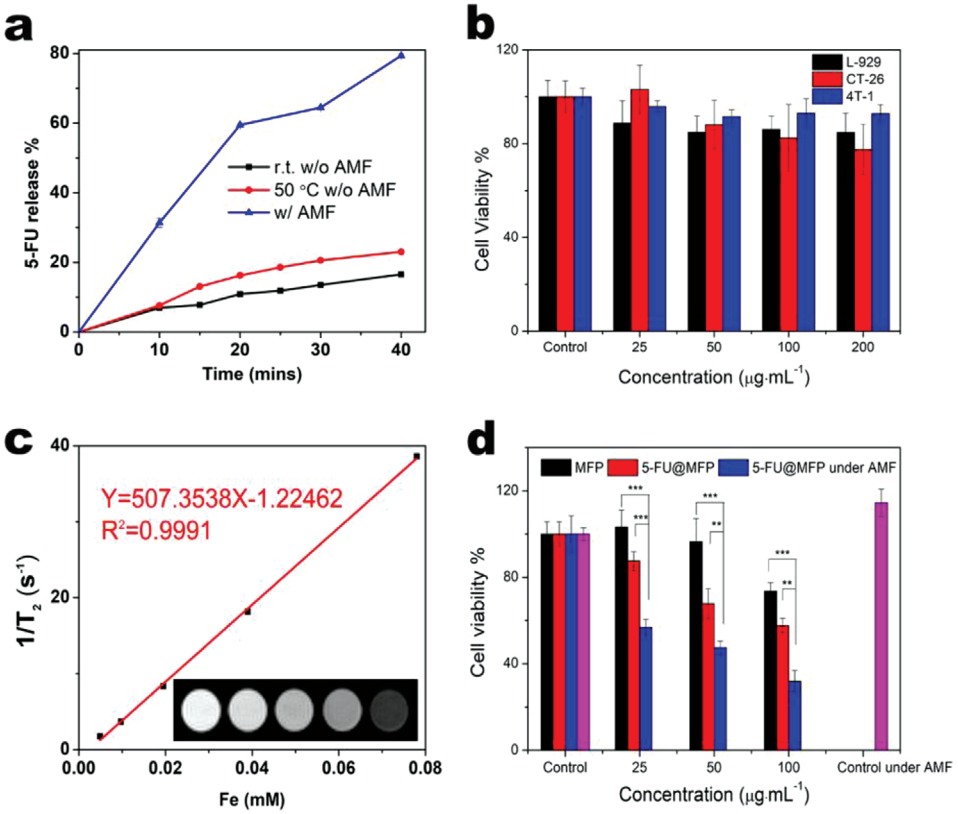

Figure 6. a) Time-dependent 5-FU release profile with and without the application of AMF (310 kHz and 800 Oe); b) cell viability of L-929, CT-26, and 4T-1 cells incubated with MFC. Data are expressed as means ± SD ($n = 5$); c) r_2 of MFC with different concentrations of [Fe] and bottom insert image shows corresponding T_2-weighted MRI (The concentration of [Fe] from left to right is 0.0049, 0.0097, 0.0195, 0.039, 0.078 mM); d) cell viability of 4T-1 cell treated with MFP and 5-FU@MFP with and without application of AMF (221 kHz and 245 Oe) for 20 min. The black bar represents cells that were incubated with MFP nanoparticles for 24 h; the red bar represents cells that were incubated with 5-FU@MFP for 24 h; The blue bar is related to cells that were incubated with 5-FU@MFP for 20 h and subjected to AMF for 20 min. Data are expressed as means ± SD ($n = 4$) and are compared by means of an unpaired students' *t*-test. ($^{*}p < 0.05$, $^{**}p < 0.01$, and $^{***}p < 0.0010$).

decreased from 92% to 81% under 400 Oe magnetic field with an increase in treatment time from 5 to 10 min. This lays a foundation to develop the following hyperthermia fields for our system.

Due to its advantage as an MTDR carrier for loading and releasing a drug, as well as its potential as a hyperthermia agent, the combination for chemo and thermo therapies could achieve a synergistic functionality for cancer cell toxicity. To make it more clinically applicable,[5,50] the equipment is modified as shown in Figure S30c (Supporting Information) with an AC magnetic field value of 245 Oe at 221 kHz. 4T-1 cells were incubated for 20 h in the presence of MFP and 5-FU@MFP, and then subjected to AMF for 20 min. From Figure 6d with the real time in vitro IR thermal imaging (Figure S31, Supporting Information), it is observed that AMF had negligible cytotoxicity to 4T-1 cell lines. The as-prepared MFP had cell viability toward 4T-1 with 74% at the concentration of 100 μg mL^{-1}. After 24 h of culture with 5-FU@MFP, the relative cell viability showed a decrease to 58% at the concentration of 100 μg mL^{-1}, suggesting that 5-FU released from MFP caused more cancer cell death.[51] Furthermore, with the application of AMF for 20 min, it shows a significant decrease of cell viability to 31% at the concentration of 100 μg mL^{-1}, as compared to MFP under AMF for 20 min with the cell viability decreasing to ≈40% at the concentration of 100 μg mL^{-1} (Figure S32, Supporting Information). It suggests that 5-FU@MFP with application of an AC magnetic field value of 245 Oe at 221 kHz could induce more cancer cell death since the local temperature at 5-FU@MFP surface is higher than the macroscopic temperature (Figure S30d, Supporting Information), resulting in both 5-FU release and hyperthermia effect. Interestingly, after 4T-1 cell treated with 5-FU for 24 h, it is observed that the cell viability was 31% at the concentration of 9.6 μg mL^{-1} (Figure S33, Supporting Information) that is equivalent to the amount of 5-FU in 100 μg mL^{-1} of 5-FU@MFP (which is determined by 5-FU loading efficiency of 13.1 wt.% in Figure S22, Supporting Information), suggesting the same percentage of cell viability as compared with 5-FU@MFP under AMF. This demonstrates that the on-demand release carrier with application of AMF could promote cancer cell death within a much shorter time as compared with the pure drug. Furthermore, the cell viability of IONP-COOH (equal amount of IONP-COOH encapsulated into MOF framework) with the application of AMF (221 kHz, 245 Oe, 20 min) was found to be almost 100%, showing the heat generated by this amount of IONP-COOH nanoparticles does not cause cell death (Figure S34, Supporting Information). The combined chemo and hyperthermia therapy effects for the on-demand carrier were also proved by the live and dead cell staining

© 2023 Wiley-VCH GmbH

16136829, 2024, 12, Downloaded from https://onlinelibrary.wiley.com/doi/10.1002/smll.202306940 by University Of Toronto Librarie, Wiley Online Library on [25/03/2024]. See the Terms and Conditions (https://onlinelibrary.wiley.com/terms-and-conditions) on Wiley Online Library for rules of use; OA articles are governed by the applicable Creative Commons License

experiment. Live and dead cells were stained by calcein-AM (green fluorescence) and propidium iodide (PI, red fluorescence), respectively. Confocal laser scanning microscopy (CLSM) was used to observe the trend in cancer cell death, showing that more cancer cells were dead when treated with 5-FU@MFP with the application of AMF (Figure S35, Supporting Information). Our materials successfully showed in vitro treatment by combining on-demand drug release and hyperthermia, as confirmed by a proof-of-concept cell study.

3. Conclusion

We successfully developed a novel MTDR nanocarrier with improved heating efficiency through implementing an innovative technique to spatially distribute and fix IONPs within a MOF matrix in a non-agglomerated manner. By grafting the MOF crystal surface with the AMF-responsive agent PNIPAM, it exhibits burst-release under AMF at the PNIPAM's collapsing state and slow-release under RT at hydrated states of the polymer. Such drug-loaded core-shell MTDR nanocomposite, with their improved heating activity, is a promising multimodal therapeutic nanoplatform for combined AMF-controlled drug delivery and hyperthermia functionalities through triggering localized heat remotely by AMF, leading to cancer cell toxicity. In addition, the MTDR carrier features high transverse relaxivity (507.35 mM^{-1} s^{-1}), holding promise for precision hyperthermia therapy that can be guided by MR thermal imaging. Moreover, our design technique is versatile, as different sizes of IONPs can be encapsulated and fixed into the MOF matrix, paving the way for its application in different magnetic nanoparticles (e.g., $Zn_{0.4}Fe_{2.6}O_4$, and exchange-coupled core/shell $CoFe_2O_4$@$MnFe_2O_4$). Our technique also offers the opportunity to modify the surface group of the magnetic nanoparticle to the coordination group of MOFs, allowing for potential assembly with various MOFs, such as MIL-101. This extension of our technique holds great promise for elevating the magneto-thermal efficiency and drug-carrying capacity[52], enabling viscous-independent SAR behaviors and drug dosing that is magneto-thermally modulated upon their delivery to tumor site through intravenous injection. These attributes make it an exciting avenue for potentially primary or adjuvant cancer treatment.

4. Experimental Section

Detailed Experimental section can be found in the Supporting Information.

Supporting Information

Supporting Information is available from the Wiley Online Library or from the author.

Acknowledgements

The authors acknowledge the Robert A. Welch Foundation (B-0027) for financial support of this work. M.H.P acknowledges support from the U.S. Department of Energy, Office of Basic Energy Sciences, Division of Materials Sciences and Engineering under Award No. DE-FG02-07ER 46438 (Magnetic and magneto-thermal studies). J.T. wants to acknowledge the financial support of the National Natural Science Foundation of China (Grant No. NSFC 21871214). Partial support from the Researchers Supporting Program (RSP2024R79) at King Saud University, Riyadh, Saudi Arabia is also acknowledged (AN). The authors thank Dr. Raja Das of Phenikaa University for his useful discussions and help with some hyperthermia experiments.

Conflict of Interest

The authors declare no conflict of interest.

Data Availability Statement

The data that support the findings of this study are available from the corresponding author upon reasonable request.

Keywords

hyperthermia treatment, iron oxide nanoparticles, magnetothermal, metal–organic frameworks, on-demand drug release

Received: August 13, 2023
Revised: November 3, 2023
Published online: December 21, 2023

[1] a) N. Kumar, M. Chaubal, A. J. Domb, R. K. N. V. Majeti, in *Encyclopedia of Polymer Science and Technology*, 3rd ed., (Ed.: H. F. Mark), Wiley, Hoboken, NJ, USA **2002**, pp. 697–720; b) C. S. Brazel, *Pharm. Res.* **2009**, *26*, 644; c) C. S. Kumar, F. Mohammad, *Adv. Drug Delivery Rev.* **2011**, *63*, 789.
[2] D. Yoo, H. Jeong, S.-H. Noh, J.-H. Lee, J. Cheon, *Angew. Chem., Int. Ed.* **2013**, *52*, 13047.
[3] a) P. Guardia, R. Di Corato, L. Lartigue, C. Wilhelm, A. Espinosa, M. Garcia-Hernandez, F. Gazeau, L. Manna, T. Pellegrino, *ACS Nano* **2012**, *6*, 3080; b) K. H. Bae, M. Park, M. J. Do, N. Lee, J. H. Ryu, G. W. Kim, C. Kim, T. G. Park, T. Hyeon, *ACS Nano* **2012**, *6*, 5266; c) E. C. Abenojar, S. Wickramasinghe, J. Bas-Concepcion, A. C. S. Samia, *Prog. Nat. Sci.: Mater. Int.* **2016**, *26*, 440; d) G. Salas, J. Camarero, D. Cabrera, H. Takacs, M. Varela, R. Ludwig, H. Dähring, I. Hilger, R. Miranda, M. D. P. Morales, F. J. Teran, *J. Phys. Chem. C* **2014**, *118*, 19985; e) G. C. Lavorato, R. Das, J. Alonso Masa, M.-H. Phan, H. Srikanth, *Nanoscale Adv.* **2021**, *3*, 867.
[4] H. Gavilán, S. K. Avugadda, T. Fernández-Cabada, N. Soni, M. Cassani, B. T. Mai, R. Chantrell, T. Pellegrino, *Chem. Soc. Rev.* **2021**, *50*, 11614.
[5] F.-C. Lin, Y. Xie, T. Deng, J. I. Zink, *J. Am. Chem. Soc.* **2021**, *143*, 6025.
[6] a) M. Lattuada, T. A. Hatton, *Langmuir* **2007**, *23*, 2158; b) S. Mourdikoudis, A. Kostopoulou, A. P. Lagrow, *Adv. Sci.* **2021**, *8*, 2004951.
[7] T. Sadhukha, T. S. Wiedmann, J. Panyam, *Biomaterials* **2014**, *35*, 7860.
[8] H. L. Ding, Y. X. Zhang, S. Wang, J. M. Xu, S. C. Xu, G. H. Li, *Chem. Mater.* **2012**, *24*, 4572.
[9] a) R. Freund, S. Canossa, S. M. Cohen, W. Yan, H. Deng, V. Guillerm, M. Eddaoudi, D. G. Madden, D. Fairen-Jimenez, H. Lyu, L. K. Macreadie, Z. Ji, Y. Zhang, B. Wang, F. Haase, C. Wöll, O. Zaremba, J. Andreo, S. Wuttke, C. S. Diercks, *Angew. Chem., Int. Ed.* **2021**, *60*, 23946; b) H. Furukawa, K. E. Cordova, M. O'keeffe, O. M. Yaghi, *Science* **2013**, *341*, 1230444; c) X. Ge, F. Jiang, M. Wang, M. Chen, Y. Li, J. Phipps, J. Cai, J. Xie, J. Ong, V. Dubovoy, J. G. Masters, L. Pan, S. Ma, *ACS Appl. Mater. Interfaces* **2023**, *15*, 677.

© 2023 Wiley-VCH GmbH

16136829, 2024, 12, Downloaded from https://onlinelibrary.wiley.com/doi/10.1002/smll.202306940 by University Of Toronto Librarie, Wiley Online Library on [25/03/2024]. See the Terms and Conditions (https://onlinelibrary.wiley.com/terms-and-conditions) on Wiley Online Library for rules of use; OA articles are governed by the applicable Creative Commons License

[10] a) P. Deria, J. E. Mondloch, O. Karagiaridi, W. Bury, J. T. Hupp, O. K. Farha, *Chem. Soc. Rev.* **2014**, *43*, 5896; b) K. Lu, T. Aung, N. Guo, R. Weichselbaum, W. Lin, *Adv. Mater.* **2018**, *30*, 1707634; c) S. Wang, C. M. Mcguirk, A. D'aquino, J. A. Mason, C. A. Mirkin, *Adv. Mater.* **2018**, *30*, 1800202.
[11] P. Horcajada, T. Chalati, C. Serre, B. Gillet, C. Sebrie, T. Baati, J. F. Eubank, D. Heurtaux, P. Clayette, C. Kreuz, J.-S. Chang, Y. K. Hwang, V. Marsaud, P.-N. Bories, L. Cynober, S. Gil, G. Férey, P. Couvreur, R. Gref, *Nat. Mater.* **2010**, *9*, 172.
[12] a) G. Lu, S. Li, Z. Guo, O. K. Farha, B. G. Hauser, X. Qi, Y. Wang, X. Wang, S. Han, X. Liu, J. S. Duchene, H. Zhang, Q. Zhang, X. Chen, J. Ma, S. C. J. Loo, W. D. Wei, Y. Yang, J. T. Hupp, F. Huo, *Nat. Chem.* **2012**, *4*, 310; b) Q. Yang, Q. Xu, H.-L. Jiang, *Chem. Soc. Rev.* **2017**, *46*, 4774; c) S. Li, F. Huo, *Nanoscale* **2015**, *7*, 7482; d) H. Liu, L. Chang, C. Bai, L. Chen, R. Luque, Y. Li, *Angew. Chem., Int. Ed.* **2016**, *55*, 1433.
[13] a) M. Aghayi-Anaraki, V. Safarifard, *Eur. J. Inorg. Chem.* **2020**, *2020*, 1916; b) X. Ge, R. Wong, A. Anisa, S. Ma, *Biomaterials* **2022**, *281*, 121322.
[14] a) M.-X. Wu, J. Gao, F. Wang, J. Yang, N. Song, X. Jin, P. Mi, J. Tian, J. Luo, F. Liang, Y.-W. Yang, *Small* **2018**, *14*, 1704440; b) H.-X. Zhao, Q. Zou, S.-K. Sun, C. Yu, X. Zhang, R.-J. Li, Y.-Y. Fu, *Chem. Sci.* **2016**, *7*, 5294; c) W. Cai, J. Wang, C. Chu, W. Chen, C. Wu, G. Liu, *Adv. Sci.* **2019**, *6*, 1801526; d) Y. Wang, J. Yan, N. Wen, H. Xiong, S. Cai, Q. He, Y. Hu, D. Peng, Z. Liu, Y. Liu, *Biomaterials* **2020**, *230*, 119619; e) F. Benyettou, G. Das, A. R. Nair, T. Prakasam, D. B. Shinde, S. K. Sharma, J. Whelan, Y. Lalatonne, H. Traboulsi, R. Pasricha, O. Abdullah, R. Jagannathan, Z. Lai, L. Motte, F. Gándara, K. C. Sadler, A. Trabolsi, *J. Am. Chem. Soc.* **2020**, *142*, 18782; f) J. Fang, Y. Yang, W. Xiao, B. Zheng, Y.-B. Lv, X.-L. Liu, J. Ding, *Nanoscale* **2016**, *8*, 3259.
[15] a) M. R. Lohe, K. Gedrich, T. Freudenberg, E. Kockrick, T. Dellmann, S. Kaskel, *Chem. Commun.* **2011**, *47*, 3075; b) S. Sene, M. T. Marcos-Almaraz, N. Menguy, J. Scola, J. Volatron, R. Rouland, J.-M. Grenèche, S. Miraux, C. Menet, N. Guillou, F. Gazeau, C. Serre, P. Horcajada, N. Steunou, *Chem* **2017**, *3*, 303.
[16] a) P. Falcaro, R. Ricco, A. Yazdi, I. Imaz, S. Furukawa, D. Maspoch, R. Ameloot, J. D. Evans, C. J. Doonan, *Coord. Chem. Rev.* **2016**, *307*, 237; b) R. Ricco, L. Malfatti, M. Takahashi, A. J. Hill, P. Falcaro, *J. Mater. Chem. A* **2013**, *1*, 13033; c) D. Wang, J. Zhou, R. Chen, R. Shi, G. Xia, S. Zhou, Z. Liu, N. Zhang, H. Wang, Z. Guo, Q. Chen, *Biomaterials* **2016**, *107*, 88; d) Y. Liu, Y. Yang, Y. Sun, J. Song, N. G. Rudawski, X. Chen, W. Tan, *J. Am. Chem. Soc.* **2019**, *141*, 7407; e) Q. Yang, Y. Zhu, B. Luo, F. Lan, Y. Wu, Z. Gu, *Nanoscale* **2017**, *9*, 527; f) F. Ke, L.-G. Qiu, J. Zhu, *Nanoscale* **2014**, *6*, 1596; g) F. Ke, L.-G. Qiu, Y.-P. Yuan, X. Jiang, J.-F. Zhu, *J. Mater. Chem.* **2012**, *22*, 9497; h) J. Chen, J. Liu, Y. Hu, Z. Tian, Y. Zhu, *Sci. Technol. Adv. Mater.* **2019**, *20*, 1043; i) X. Wang, J. Xu, D. Yang, C. Sun, Q. Sun, F. He, S. Gai, C. Zhong, C. Li, P. Yang, *Chem. Eng. J.* **2018**, *354*, 1141; j) Y. Chen, Z. Xiong, L. Peng, Y. Gan, Y. Zhao, J. Shen, J. Qian, L. Zhang, W. Zhang, *ACS Appl. Mater. Interfaces* **2015**, *7*, 16338; k) Z. Yuan, L. Zhang, S. Li, W. Zhang, M. Lu, Y. Pan, X. Xie, L. Huang, W. Huang, *J. Am. Chem. Soc.* **2018**, *140*, 15507.
[17] M. He, J. Zhou, J. Chen, F. Zheng, D. Wang, R. Shi, Z. Guo, H. Wang, Q. Chen, *J. Mater. Chem. B* **2015**, *3*, 9033.
[18] a) A. Riedinger, P. Guardia, A. Curcio, M. A. Garcia, R. Cingolani, L. Manna, T. Pellegrino, *Nano Lett.* **2013**, *13*, 2399; b) L. Polo-Corrales, C. Rinaldi, *J. Appl. Phys.* **2012**, *111*, 07B334; c) H. L. Rodríguez-Luccioni, M. Latorre-Esteves, J. Méndez-Vega, O. Soto, A. R. Rodríguez, C. Rinaldi, M. Torres-Lugo, *Int. J. Nanomed.* **2011**, *6*, 373.
[19] X.-Q. Zhan, X.-Y. Yu, F.-C. Tsai, N. Ma, H.-L. Liu, Y. Han, L. Xie, T. Jiang, D. Shi, Y. Xiong, *Crystals* **2018**, *8*, 250.
[20] J. Park, K. An, Y. Hwang, J.-G. Park, H.-J. Noh, J.-Y. Kim, J.-H. Park, N.-M. Hwang, T. Hyeon, *Nat. Mater.* **2004**, *3*, 891.
[21] Z. Chen, H. Chen, H. Hu, M. Yu, F. Li, Q. Zhang, Z. Zhou, T. Yi, C. Huang, *J. Am. Chem. Soc.* **2008**, *130*, 3023.
[22] L. Liu, Z. Chen, J. Wang, D. Zhang, Y. Zhu, S. Ling, K.-W. Huang, Y. Belmabkhout, K. Adil, Y. Zhang, B. Slater, M. Eddaoudi, Y. Han, *Nat. Chem.* **2019**, *11*, 622.
[23] a) Z. Nedelkoski, D. Kepaptsoglou, L. Lari, T. Wen, R. A. Booth, S. D. Oberdick, P. L. Galindo, Q. M. Ramasse, R. F. L. Evans, S. Majetich, V. K. Lazarov, *Sci. Rep.* **2017**, *7*, 45997; b) Z. Ma, J. Mohapatra, K. Wei, J. P. Liu, S. Sun, *Chem. Rev.* **2023**, *123*, 3904.
[24] X. Sun, N. Frey Huls, A. Sigdel, S. Sun, *Nano Lett.* **2012**, *12*, 246.
[25] A. Karmakar, P. G. M. Mileo, I. Bok, S. B. Peh, J. Zhang, H. Yuan, G. Maurin, D. Zhao, *Angew. Chem., Int. Ed.* **2020**, *59*, 1096.
[26] D. J. Denmark, J. Bradley, D. Mukherjee, J. Alonso, S. Shakespeare, N. Bernal, M. H. Phan, H. Srikanth, S. Witanachchi, P. Mukherjee, *RSC Adv.* **2016**, *6*, 5641.
[27] E. Yu, A. Lo, L. Jiang, B. Petkus, N. Ileri Ercan, P. Stroeve, *Colloids Surf., B* **2017**, *149*, 297.
[28] a) A. Baeza, E. Guisasola, E. Ruiz-Hernández, M. Vallet-Regí, *Chem. Mater.* **2012**, *24*, 517; b) E. Guisasola, A. Baeza, M. Talelli, D. Arcos, M. Moros, J. M. de la Fuente, M. Vallet-Regí, *Langmuir* **2015**, *31*, 12777.
[29] a) H. Sun, B. Tang, P. Wu, *ACS Appl. Mater. Interfaces* **2017**, *9*, 21473; b) K. A. McDonald, J. I. Feldblyum, K. Koh, A. G. Wong-Foy, A. J. Matzger, *Chem. Commun.* **2015**, *51*, 11994; c) K. Xie, Q. Fu, Y. He, J. Kim, S. J. Goh, E. Nam, G. G. Qiao, P. A. Webley, *Chem. Commun.* **2015**, *51*, 15566; d) H. Liu, H. Zhu, S. Zhu, *Macromol. Mater. Eng.* **2015**, *300*, 191.
[30] Q. Fu, G. V. R. Rao, L. K. Ista, Y. Wu, B. P. Andrzejewski, L. A. Sklar, T. L. Ward, G. P. López, *Adv. Mater.* **2003**, *15*, 1262.
[31] S. Nagata, K. Kokado, K. Sada, *Chem. Commun.* **2015**, *51*, 8614.
[32] P. Hugounenq, M. Levy, D. Alloyeau, L. Lartigue, E. Dubois, V. Cabuil, C. Ricolleau, S. Roux, C. Wilhelm, F. Gazeau, R. Bazzi, *J. Phys. Chem. C* **2012**, *116*, 15702.
[33] C. Tao, Y. Zhu, *Dalton Trans.* **2014**, *43*, 15482.
[34] J. Cai, Y. Q. Miao, B. Z. Yu, P. Ma, L. Li, H. M. Fan, *Langmuir* **2017**, *33*, 1662.
[35] Y. Wang, L. Li, P. Dai, L. Yan, L. Cao, X. Gu, X. Zhao, *J. Mater. Chem. A* **2017**, *5*, 22372.
[36] T. Zhang, X. Zhang, X. Yan, L. Kong, G. Zhang, H. Liu, J. Qiu, K. L. Yeung, *Chem. Eng. J.* **2013**, *228*, 398.
[37] Z. Nemati, J. Alonso, I. Rodrigo, R. Das, E. Garaio, J. Á. García, I. Orue, M.-H. Phan, H. Srikanth, *J. Phys. Chem. C* **2018**, *122*, 2367.
[38] Q. K. Ong, A. Wei, X.-M. Lin, *Phys. Rev. B* **2009**, *80*, 134418.
[39] K. L. Krycka, J. A. Borchers, R. A. Booth, Y. Ijiri, K. Hasz, J. J. Rhyne, S. A. Majetich, *Phys. Rev. Lett.* **2014**, *113*, 147203.
[40] E. Yu, I. Galiana, R. Martínez-Mánez, P. Stroeve, M. D. Marcos, E. Aznar, F. Sancenón, J. R. Murguía, P. Amorós, *Colloids Surf., B* **2015**, *135*, 652.
[41] A. Ramachandra Kurup Sasikala, R. G. Thomas, A. R. Unnithan, B. Saravanakumar, Y. Y. Jeong, C. H. Park, C. S. Kim, *Sci. Rep.* **2016**, *6*, 20543.
[42] S. K. Hekmatyar, R. M. Kerkhoff, S. K. Pakin, P. Hopewell, N. Bansal, *Int. J. Hyperthermia* **2005**, *21*, 561.
[43] R. T. Gordon, J. R. Hines, D. Gordon, *Med. Hypotheses* **1979**, *5*, 83.
[44] X. Gao, M. Zhai, W. Guan, J. Liu, Z. Liu, A. Damirin, *ACS Appl. Mater. Interfaces* **2017**, *9*, 3455.
[45] R. A. Al-Thawabeia, H. A. Hodali, *J. Chem.* **2015**, *2015*, 1.
[46] M. Peller, K. Böll, A. Zimpel, S. Wuttke, *Inorg. Chem. Front.* **2018**, *5*, 1760.
[47] E. A. Neuwelt, C. G. Várallyay, S. Manninger, D. Solymosi, M. Haluska, M. A. Hunt, G. Nesbit, A. Stevens, M. Jerosch-Herold, P. M. Jacobs, J. M. Hoffman, *Neurosurgery* **2007**, *60*, 601.
[48] K. C. Barick, M. Aslam, Y.-P. Lin, D. Bahadur, P. V. Prasad, V. P. Dravid, *J. Mater. Chem.* **2009**, *19*, 7023.

© 2023 Wiley-VCH GmbH

16136829, 2024, 12, Downloaded from https://onlinelibrary.wiley.com/doi/10.1002/smll.202306940 by University Of Toronto Librarie, Wiley Online Library on [25/03/2024]. See the Terms and Conditions (https://onlinelibrary.wiley.com/terms-and-conditions) on Wiley Online Library for rules of use; OA articles are governed by the applicable Creative Commons License

[49] a) V. Agostoni, P. Horcajada, M. Noiray, M. Malanga, A. Aykaç, L. Jicsinszky, A. Vargas-Berenguel, N. Semiramoth, S. Daoud-Mahammed, V. Nicolas, C. Martineau, F. Taulelle, J. Vigneron, A. Etcheberry, C. Serre, R. Gref, *Sci. Rep.* **2015**, *5*, 7925; b) X. Chen, Y. Zhuang, N. Rampal, R. Hewitt, G. Divitini, C. A. O'keefe, X. Liu, D. J. Whitaker, J. W. Wills, R. Jugdaohsingh, J. J. Powell, H. Yu, C. P. Grey, O. A. Scherman, D. Fairen-Jimenez, *J. Am. Chem. Soc.* **2021**, *143*, 13557.
[50] J. Pan, Y. Xu, Q. Wu, P. Hu, J. Shi, *J. Am. Chem. Soc.* **2021**, *143*, 8116.
[51] M. Prabaharan, J. J. Grailer, D. A. Steeber, S. Gong, *Macromol. Biosci.* **2009**, *9*, 744.
[52] a) W. Wu, J. Liu, X. Lin, Z. He, H. Zhang, L. Ji, P. Gong, F. Zhou, W. Liu, *J. Colloid Interface Sci.* **2023**, *644*, 200; b) W. Wu, J. Liu, P. Gong, Z. Li, C. Ke, Y. Qian, H. Luo, L. Xiao, F. Zhou, W. Liu, *Small* **2022**, *18*, 2202510.

 © 2023 Wiley-VCH GmbH

16136829, 2024, 12, Downloaded from https://onlinelibrary.wiley.com/doi/10.1002/smll.202306940 by University Of Toronto Librarie, Wiley Online Library on [25/03/2024]. See the Terms and Conditions (https://onlinelibrary.wiley.com/terms-and-conditions) on Wiley Online Library for rules of use; OA articles are governed by the applicable Creative Commons License